AD-A188 147 ICE-SHELF RESPONSE TO ICE-STREAM DISCHARGE FLUCTUATION: 1/1
I UNCONFINED ICE TONGUES(U) CHICAGO UNIV IL DEPT OF
GEOPHYSICAL SCIENCES D R MACAYEAL ET AL 1987
UNCLASSIFIED N00014-86-K-0034 F/G 8/12 NL

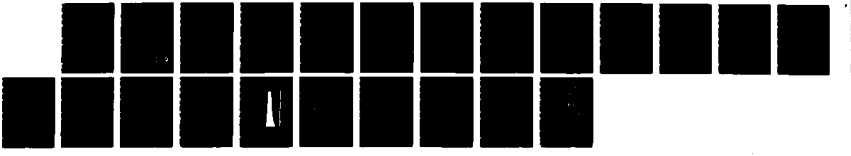

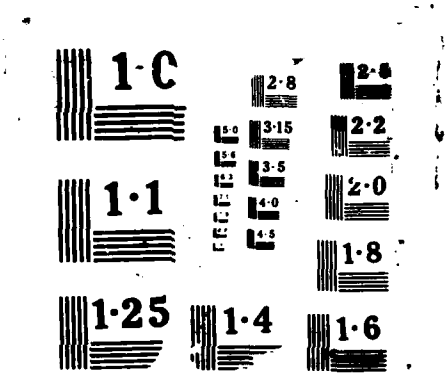
1·C
1·1
1·25
1·4
2·8
3·15
3·5
4·0
4·5
2·8
2·2
2·0
1·8
1·6

(12)

Ice-shelf response to ice-stream discharge fluctuation: I. unconfined ice tongues.

Douglas R. MacAyeal

and

Victor Barcilon

Department of Geophysical Sciences
The University of Chicago
5734 South Ellis Avenue
Chicago, Illinois 60637

Contract N00014-86-K-0034

Abstract

Ice-stream discharge fluctuations constitute an independent means of forcing unsteady ice-shelf behavior, and their effect must be distinguished from those of oceanic and atmospheric climate to understand ice-shelf change. Ice-stream-generated fluctuations of a one-dimensional ice shelf are found here to propagate through the ice-shelf environment along the two characteristics of the hyperbolic governing equations. One characteristic permits instantaneous transmission of grounding-line velocity changes to all points downstream. The other characteristic represents slow transmission of grounding-line thickness changes along Lagrangian particle paths.

Introduction

Unsteady thickness and flow observed on the Ross Ice Shelf are thought to result primarily from fluctuations of ice streams and outlet glaciers that feed the ice shelf at its inland boundaries (Shabtaie and Bentley, 1987; MacAyeal and others, *in press*). The initial effects of climatic change thus must be discriminated from an ever-present background of ice-stream-generated variability. To characterize this variability, we determine the general characteristics of ice-thickness and flow anomalies produced by time-varying grounding-line discharge. We restrict our examination to anomalies of an ideal, floating ice tongue to facilitate and analytic treatment of the governing equations. Our results provide: (i) a conceptual basis for modeling thickness and flow variations of West Antarctic ice shelves (such as developed in a companion paper, MacAyeal and Lange, *unpublished*), and (ii) an understanding of how inland-ice discharge may compete with oceanic and atmospheric conditions to force such variations.

Characteristic Equations

Thickness $H(x,t)$ and longitudinal velocity $U(x,t)$ for the ideal ice-shelf geometry ($x>0$) shown in Figure 1 satisfy

$$\partial_t H + U\partial_x H = M - A^n H^{n+1} \qquad (1)$$

$$\partial_x U = A^n H^n \qquad (2)$$

subject to boundary conditions (specifying H and u as functions of time) at the grounding line $x=0$ (note, ∂_x denotes the x-derivative, etc.). Equations 1 and 2 are derived in the Appendix and stem from mass-continuity and stress-equilibrium principles, subject to certain simplifying assumptions. Dimensionless variables are defined in Table I using scales typical of Antarctic conditions (Holdsworth, 1985).

Steady-state solutions to Equations 1 and 2, $H_s(x)$ and $U_s(x)$, satisfying $H_s(0)=1$ and $U_s(0)=1$ at the grounding line were found by Van der Veen (1983) and are written (for $M>0$):

$$H_s(x) = [(1-\gamma)/(1+Mx)^{n+1} + \gamma]^{(-1/(n+1))} \quad (3)$$

$$U_s(x) = [1 - \gamma + \gamma(1+Mx)^{n+1}]^{(1/(n+1))} \quad (4)$$

where $\gamma=A^n/M$. $H_s(x)$ monotonically decreases with increasing distance from the grounding line and approaches a constant value $\gamma^{-1/(n+1)}$ as $x\rightarrow\infty$. This asymptotic thickness (approximately 200 m for typical Antarctic conditions) is achieved because ice-shelf thinning by horizontal spreading is balanced by snow accumulation M. $U_s(x)$ monotonically increases with distance from the grounding line, but does not approach an asymptotic limit as $x\rightarrow\infty$.

Deviations from steady state caused by fluctuations in H and u at the grounding line can be computed directly from Equations 1 and 2. Alternative forms of Equations 1 and 2, called the characteristic equations, are useful, however, for displaying fundamental properties of the solution. They are derived by defining new spatial and temporal coordinates that produce ordinary differential equations for thickness and velocity (the method of characteristics) and are written:

$$\partial_\tau x - U\partial_\tau t = 0 \quad (5)$$

$$\partial_\xi t = 0 \quad (6)$$

$$\partial_\tau H - (M-A^nH^{n+1})\partial_\tau t = 0 \quad (7)$$

$$\partial_\xi U - A^nH^n\partial_\xi x = 0 \quad (8)$$

where $H(\xi,\tau)$ and $U(\xi,\tau)$ represent thickness and velocity, respectively, as functions of alternative coordinates ξ and τ that satisfy

$$\partial_t\xi + U\partial_x\xi = 0 \quad (9)$$

$$\partial_x\tau = 0 \quad (10)$$

The curves $\xi = \xi_o$ and $\tau = \tau_o$ in the x,t plane represent characteristics of the ice-shelf system along which changing conditions propagate. These curves can be determined by solving Equations 5 and 6 for $x(\xi,\tau)$ and $t(\tau)$ (t and τ can be taken as identical in the present application; this gives $\partial_\tau t = 1$). As shown by Equation 5, the characteristic $\xi = \xi_o$ represents the trajectory of a particular ice column (which may be labeled by its ξ-coordinate ξ_o) in the x,t plane. The thickness of this particular ice column, $H(\xi=\xi_o,\tau)$, is determined as a function of τ by Equation 7. The velocity of this ice column, $U(\xi=\xi_o,\tau)$, is found by integrating Equation 8 over the domain $\xi_1(\tau)<\xi<\xi_o$ where $\xi_1(\tau)$ is the ξ-label of the ice column currently at the grounding line. This interval, in x-coordinates, spans the distance between the grounding line and $x = x(\xi_o,\tau)$.

The characteristic equations illuminate several basic aspects of time-dependent ice-shelf adjustment. Equation 7 indicates that the thickness of a given ice column (ξ=constant) evolves independently of the ice thickness elsewhere. This independence is an aspect of unconfined ice shelves only. In circumstances where coastal confinement introduces resistance to seaward flow, evolution of a given ice column depends on thickness conditions downstream.

Another basic aspect of ice-shelf behavior illuminated by Equations 7 and 8 is that deviations from steady-state are limited in space and time by the appropriate characteristic curves. If, for example, H or U at x=0 are impulsively changed at t=0 and the initial conditions are in steady state, unsteady conditions will prevail only within the region of the x,t plane bounded ty the curves ξ=constant and τ=constant that emanate from x=t=0. This partition of the x,t plane

into steady and unsteady regions is shown schematically in Figure 2. Change propagates downstream instantaneously along the τ=constant curve because velocity at any point is determined by spatial integration of the instantaneous ice-thickness distribution. Equilibration with new forcing conditions is completed, however, in a delayed fashion following the ξ=constant curve. Steady-state conditions prevail in the wake of the ice column that was at the grounding line at the instant t=0. This ice column follows the path determined by the ξ=constant characteristic.

Transient Ice-Shelf Profiles

We demonstrate basic ice-shelf response by computing ice thickness and velocity anomalies generated by prescribed scenarios of unsteady grounding-line discharge. These anomalies are defined by

$$h(x,t) = H(x,t) - H_s(x) \tag{11}$$

$$u(x,t) = U(x,t) - U_s(x) \tag{12}$$

where $H_s(x)$ and $U_s(x)$ are the steady-state thickness and velocity profiles defined by Equations 3 and 4, respectively. To simplify the calculations, we require h and u to be small and use a linear expansion of Equations 1 and 2:

$$\partial_t h + U_s \partial_x h = -(n+1)A^n H_s^n h - \partial_x H_s u \tag{13}$$

$$\partial_x u = nA^n H_s^{n-1} h \tag{14}$$

With this simplification, the two generic characteristic curves ξ=constant and τ=constant associated with steady-state conditions may be applied as approximations to the characteristic curves associated with unsteady conditions.

Boundary conditions at the grounding line (x=0) and initial conditions are specified to represent three basic scenarios of ice-stream discharge fluctuations (amplitudes and time constants are

arbitrary for demonstration):

$$\text{scenario I} - \begin{cases} u(x,0) = h(x,0) = 0.0 & \\ u(0,t) = h(0,t) = 0.1 & 0 \le t \le 0.2 \\ 0.0 & t > 0.2 \end{cases} \tag{15}$$

$$\text{scenario II} - \begin{cases} h(0,t) = 0.1 \sin(\omega t) \\ u(0,t) = 0.0 \end{cases} \tag{16}$$

$$\text{scenario III} - \begin{cases} h(0,t) = 0.0 \\ u(0,t) = 0.1 \sin(\omega t) \end{cases} \tag{17}$$

where $\omega = 2\pi/0.5$. Scenario I represents an episode of increased grounding-line thickness and velocity that is sustained for a brief time interval. Scenarios II and III represent periodic fluctuations in h and u (we do not consider a variety of forcing frequencies in the present study; see, however, MacAyeal and Lange, *unpublished*). Initial conditions for scenarios II and III are not required because the grounding line forcing is assumed to proceed *ad infinitum* (in practice, we apply an initial condition of $h(x,0)=0$ and $u(x,0)=0$, and proceed with time integration until all manifestations of the initial conditions have dissipated).

Finite-difference solutions to Equations 13 and 14 under the three forcing scenarios described above were produced on the interval $0 \le x \le 1$ and over a sufficient time interval to display salient features (and to dissipate transients induced by initial conditions in periodic forcing scenarios). The finite-difference form of Equation 13 possessed implicit time steps ($\Delta t = 0.01$) and centered space derivatives ($\Delta x = 0.01$), except at $x = 1.0$ where an upwind space derivative was used. Equation 14

was integrated at each time step over x using centered space derivatives (except upwind at x=1.0).

Salient features of scenario I are displayed by the contour maps of thickness anomaly h and volume flux anomaly q, defined by

$$q(x,t) = u(x,t)H_s(x) + h(x,y,t)U_s(x) \qquad (18)$$

in Figure 3. In Figure 4, the x,t plane on which these maps are presented is divided into five regions by the four characteristic curves that emanate from the grounding line at the start and end of the modified discharge episode. In regions I, III and V shown in Figure 3, ice-shelf conditions are in steady state with current discharge thickness and velocity [$H_s(0)$ + $h(0,t)$ and $U_s(0)$ +$u(0,t)$]. In regions II and IV, conditions are unsteady. Comparison of the maps of h and q indicates that thickness anomalies are organized primarily along ξ=constant trajectories and that flux anomalies tend to display rapid, discontinuous changes along τ=constant trajectories.

Ice-thickness anomalies generated in response to scenarios II and III (periodic forcing) indicate two contrasting patterns shown in Figure 5. For oscillatory grounding-line thickness (scenario II), h is maximum at the grounding line and decay monotonically downstream. Ridges and troughs of the $h(x,t)$ contours in the x,t plane for this situation extend along ξ=constant trajectories. In contrast, the maximum of h generated by scenario III (oscillatory grounding line velocity) occurs downstream of the grounding line at a location that depends on the frequency of forcing (the lower the frequency, the farther downstream).

Comparison of scenarios II and III suggests that phase relationships between thickness and velocity oscillations of a given ice

stream is critical in determining the location of maximum ice thickness anomalies on the ice shelf. This aspect of ice-stream dynamics may thus determine where ice rumples and rises are likely to form in response to ice-stream changes.

Conclusion

Discrimination between ice-stream and climatically forced ice-shelf transience can be accomplished through the relationship between ice-shelf anomalies and the characteristic trajectories that determine propagation of ice-shelf change. Variability forced by the atmosphere or ocean would not necessarily be constrained to propagate along such characteristics, but may propagate through the ice-shelf environment along pathways determined by oceanic and atmospheric dynamics.

The two types of characteristics described represent fast and slow paths by which grounding-line influences are transmitted to the ice shelf downstream. Velocity and mass-flux changes are propagated instantaneously via the fast path because the velocity profile is determined by an elliptic boundary-value operator. Thickness changes are propagated advectively via the slow path because ice-column thickness evolves (in an unconfined ice shelf) independently of ice-column conditions elsewhere.

This research was supported by the National Science Foundation (DPP 85 09451) and the Office of Naval Research under Grant N00014-86-K-0034. We thank L. Morland for productive discussions at the University of Chicago in December, 1986.

Appendix: Derivation of Governing Equations

Mass balance, stress equilibrium, heat-flow continuity and the material properties of ice govern the evolution of large ice masses. For ice shelves that float on an effectively frictionless ocean, and that span a horizontal distance greater than their thickness, these principles are considerably simplified in that vertical variation of the horizontal flow is negligible. This simplification has been demonstrated by a number of means (Sanderson and Doake, 1979; Morland, 1987; and Muszynski and Birchfield, 1987), and is generally supported by observation. In the present study, we justify this simplification and derive the governing equations for the ideal ice-shelf configuration we consider by expanding the stress-equilibrium equations and associated boundary conditions using δ^2 (the square of the aspect ratio). We conduct this derivation under the assumption that temperature-dependent rheological parameters may be replaced with similar depth-dependent parameters to approximate the prevalent vertical temperature gradient in Antarctic ice shelves. More precise treatment of thermo-mechanical coupling (such as demonstrated by Williams and Hutter, 1983; Shumskiy and Krass, 1979; or Morland and Shoemaker, 1982) is not necessary to achieve the limited objectives of this study. We additionally restrict our analysis to two dimensions (vertical and horizontal along the longitudinal axis).

Stress equilibrium in the horizontal (x) and vertical (z) directions, and dynamic boundary conditions at the ice shelf surface ($z_s(x)$, stress free) and base ($z_b(x)$, sea-water pressure only), are written:

$$-\Gamma\partial_x P + \partial_x(\nu e_{xx}) + \delta^{-2}\partial_z(\nu e_{xz}) = 0 \qquad z_b<z<z_s \qquad (a1)$$

$$-\Gamma\partial_z P + \partial_x(\nu e_{xz}) + \partial_z(\nu e_{zz}) - \Gamma = 0 \qquad z_b<z<z_s \qquad (a2)$$

$$-\partial_x z_s(\nu e_{xx} - \Gamma P) + \delta^{-2}\nu e_{xz} = 0 \qquad z=z_s \qquad (a3)$$

$$-\partial_x z_s \nu e_{xz} + \nu e_{zz} - \Gamma P = 0 \qquad z=z_s \qquad (a4)$$

$$\partial_x z_b(\nu e_{xx} - \Gamma P) - \delta^{-2}\nu e_{xz} = (\rho_w/\rho_i)\Gamma\partial_x(\tfrac{1}{2}z_b^2) \qquad z=z_b \qquad (a5)$$

$$\partial_x z_b \nu e_{xz} - \nu e_{zz} + \Gamma P = -(\rho_w/\rho_i)\Gamma z_b \qquad z=z_b \qquad (a6)$$

where we have replaced reference to the deviatoric stress using

$$T_{ij}' = 2\nu e_{ij} \qquad (a7)$$

and the effective viscosity υ is defined so as to represent Glen's flow law

$$\nu = B(z)/[(\tfrac{1}{2}(e_{xx}^2 + e_{zz}^2 + 2e_{xz}^2))^{\frac{1}{2}-1/(2n)}] \qquad (a8)$$

All variables are defined in Table I and are expressed in non-dimensional form (Hutter, 1983). As stated above, the non-dimensional flow-law parameter B(z) is assumed z-dependent, rather than temperature-dependent, to avoid the need to treat thermo-mechanical coupling.

Systematic approximations to Equations a1 - a6 are developed by expanding all variables in power series using the small parameter δ^2. The zero-order approximations to Equations a1 - a6 are

$$\partial_z(\nu^{(0)} e_{xz}^{(0)}) = 0 \qquad z_b^{(0)}<z<z_s^{(0)} \qquad (a9)$$

$$-\Gamma\partial_z P^{(0)} + \partial_x(\nu^{(0)} e_{xz}^{(0)}) + \partial_z(\nu^{(0)} e_{zz}^{(0)}) - \Gamma = 0 \qquad z_b^{(0)}<z<z_s^{(0)} \qquad (a10)$$

$$\nu^{(0)} e_{xz}^{(0)} = 0 \qquad z=z_s^{(0)} \qquad \text{(a11)}$$

$$-\partial_x z_s^{(0)} \nu^{(0)} e_{xz}^{(0)} + \nu^{(0)} e_{zz}^{(0)} - \Gamma p^{(0)} = 0 \qquad z=z_s^{(0)} \qquad \text{(a12)}$$

$$\nu^{(0)} e_{xz}^{(0)} = 0 \qquad z=z_b^{(0)} \qquad \text{(a13)}$$

$$\partial_x z_b^{(0)} \nu^{(0)} e_{xz}^{(0)} - \nu^{(0)} e_{zz}^{(0)} + \Gamma p^{(0)} = -(\rho_w/\rho_i)\Gamma z_b^{(0)} \qquad z=z_b^{(0)} \qquad \text{(a14)}$$

The zero-order solution can be obtained immediately by integrating Equations a9 and a10 subject to the boundary conditions a11 - a14:

$$e_{xz}^{(0)} = 0 \qquad \text{(a15)}$$

$$p^{(0)} = (z_s^{(0)} - z) + (\nu^{(0)}/\Gamma)\, e_{zz}^{(0)} \qquad \text{(a16)}$$

$$z_b^{(0)} = \rho_i/(\rho_i - \rho_w)\, z_s^{(0)} \qquad \text{(a17)}$$

The above solutions indicate that: (i) vertical shear in the ice column is negligible, (ii) pressure increases linearly with depth, and (iii) the ice shelf floats in local hydrostatic equilibrium.

A subset of the first-order approximations to Equations a1 - a6 (for the x-component of forces) describes how the zero-order strain rate $e_{xx}^{(0)}=-e_{zz}^{(0)}$ varies with $H^{(0)}=z_s^{(0)}-z_b^{(0)}$:

$$\partial_z \nu^{(0)} e_{xz}^{(1)} = \Gamma \partial_x p^{(0)} - \partial_x (\nu^{(0)} e_{xx}^{(0)}) \qquad z_b^{(0)}<x<z_s^{(0)} \qquad \text{(a18)}$$

$$\nu^{(0)} e_{xz}^{(1)} = \partial_x z_s^{(0)} (\nu^{(0)} e_{xx}^{(0)} - \Gamma p^{(0)}) \qquad z=z_s^{(0)} \qquad \text{(a19)}$$

$$\nu^{(0)} e_{xz}^{(1)} = \partial_x z_b^{(0)} (\nu^{(0)} e_{xx}^{(0)} - \Gamma p^{(0)} - \rho_w/\rho_i \Gamma z_b^{(0)}) \quad z=z_b^{(0)} \qquad \text{(a20)}$$

Integration of Equation a18 over z using boundary conditions a19 and a20 followed by integration of the result over x (assuming that $e_{xx}^{(0)} \to 0$ as $H^{(0)} \to 0$, and that Γ, ρ_w and ρ_i are independent of x) gives

$$\bar{\nu}^{z\,(0)} e_{xx}^{(0)} = \tfrac{1}{4} \Gamma \, (1-\rho_i/\rho_w) \, H^{(0)} \qquad \text{(a21)}$$

where

$$\bar{\nu}^{z\,(0)} = \int_{z_b}^{z_s} B(z') \, dz' \; / \; (e_{xx}^{(0)\;1-1/n}) \qquad \text{(a22)}$$

Substitution of Equation a22 into a21 gives

$$e_{xx}^{(0)} = \partial_x U = A^n H^n \qquad \text{(a24)}$$

where

$$A = \tfrac{1}{4} \Gamma / B^z \, (1 - \rho_i/\rho_w) \qquad \text{(a25)}$$

is a non-dimensional parameter that measures the ratio of the gravitationally driven spreading stress to the stress required to deform the ice shelf at the chosen strain-rate scale U_o/L_o.

References

Holdsworth, G. 1985. Some effects of ocean currents and wave motion on the dynamics of floating glacier tongues. (In *Oceanology of the Antarctic Continental Shelf*. S.S. Jacobs, editor. Antarctic Research Series, Vol 43. p. 253-71, American Geophysical Union, Washington).

Hutter, K. 1983. *Theoretical Glaciology*. D. Reidel, Dordrecht.

MacAyeal, D.R. and others. *in press*. Force, mass and energy budgets of the Crary Ice-Rise complex, Antarctica. *by* D.R. MacAyeal, R.A. Bindschadler, S. Shabtaie, S. Stephenson and C.R. Bentley. *Journal of Glaciology*, Vol. , No. , p. .

MacAyeal, D.R. and Lange, M.A. *unpublished*. Ice-shelf response to transient ice-stream discharge: II. single ice stream discharging into a rectangular ice shelf. submitted to *Journal of Glaciology* as a companion paper.

Morland, L.W. 1987. Unconfined ice-shelf flow. (In *Dynamics of the West Antarctic Ice Sheet*. C.J. van der Veen and J. Oerlemans, editors. p. 99-116, D. Reidel, Dordrecht).

Morland, L.W. and Shoemaker, E.M. 1982. Ice shelf balances. *Cold Regions Science and Technology*, Vol. 5, p. 235-51.

Muszynski, I. and Birchfield, G.E. 1987. A coupled marine ice-stream-ice-shelf model. *Journal of Glaciology*, Vol. 33, No. 113, p. 3-16.

Sanderson, T.J.O. and Doake, C.S.M. 1979. Is vertical shear in an ice shelf negligible? *Journal of Glaciology*, Vol. 22, No. 87, p. 285-92.

Shabtaie, S. and Bentley, C.R. 1987. West Antarctic ice streams draining into the Ross Ice Shelf: Configuration and mass balance. *Journal of Geophysical Research*, Vol. 92, No. B2, p. 1311-36.

Shumskiy, P.A. and Krass, M.S. 1976. Mathematical models of ice shelves. *Journal of Glaciology*, Vol. 17, No. 77, p. 419-32.

van der Veen, C.J. 1983. A note on the equilibrium profile of a free floating ice shelf. *Technical Report*. Instituut voor Meteorologie en Oceanografie, Rijksuniversiteit, Utrecht, Vol. 83, No. 15.

Williams, F.M. and Hutter, K. 1983. Thermal response of unconfined ice shelves to climatic conditions. *Acta Mechanica*, Vol. 48, p. 131-46.

Table I - Variables and scales

Variable	Definition	Units	Scale	
			Symbol	Value
H	Ice thickness	m	H_o	10^3
U	horizontal velocity	m/s	U_o	1.58×10^{-5}
h	thickness anomaly	m	H_o	10^3
u	velocity anomaly	m/s	U_o	1.58×10^{-5}
ξ	characteristic coordinate	m	L_o	10^4
τ	characteristic coordinate	s	L_o/U_o	6.33×10^8
x	horizontal coordinate	m	L_o	10^4
z	vertical coordinate	m	H_o	10^3
δ	aspect ratio	-	H_o/L_o	10^{-1}
t	time	s	L_o/U_o	6.33×10^8
M	accumulation rate	m/s	U_oH_o/L_o	7.92×10^{-9}
ρ_i	ice density	kg/m^3	ρ_i	917
g	gravity	m/s^2	g	9.81
ρ_w	sea-water density	kg/m^3	ρ_w	1028
B_o	flow-law constant	Pa s$^{-1/n}$	B_o	1.5×10^8
n	flow-law exponent		3	
A	stress ratio		$\dfrac{\rho g H_o(1-\rho/\rho_w)}{4(U_o/L_o)^{1/n}B_o}$	1.39
p	pressure	Pa	$\rho_i g H_o$	9.0×10^6
e_{xx}	longitudinal strain rate	s^{-1}	U_o/L_o	1.58×10^{-9}
e_{zz}	vertical strain rate	s^{-1}	U_o/L_o	1.58×10^{-9}
e_{xz}	vertical shear rate	s^{-1}	U_o/L_o	1.58×10^{-8}
υ	effective viscosity	Pa s	$Bo/\{2(U_o/L_o)^{1-1/n}\}$	5.5×10^{13}
T'_{ij}	deviatoric stress	Pa	$\rho g H_o$	9.0×10^6
z_s	surface elevation	m	H_o	10^3
z_b	basal depth	m	H_o	10^3
Γ	stress ratio	non-dimensional	$\rho g H_o/\{B_o(U_o/L_o)^{1/n}\}$	51.4

Figure Captions

Figure 1. Cross section of ideal ice shelf considered in this study. The trajectory of the ice column labeled ξ_o follows one of the two types of characteristics associated with the governing equations. If ice-stream discharge was impulsively changed between two otherwise steady conditions at the time this ice column was at the grounding line, the subsequent locations of this ice column will separate the region where steady-state conditions have been renewed (upstream) from the region where adjustment is still underway (downstream).

Figure 2. If ice-stream discharge (grounding line thickness and velocity) is changed impulsively at t=0, unsteady conditions will prevail only within the region of the x,t plane bounded by the ξ=constant and τ=constant characteristics.

Figure 3. Ice thickness (top) and flux (bottom) anomalies (non-dimensional units, Table I) resulting from a limited episode of modified ice-stream discharge (scenario I). The ranges of x and t displayed above are both 0.0→1.0 (non-dimensional units). Comparison with the characteristics shown in Figure 4 suggests that thickness anomalies primarily follow ξ=constant characteristics; whereas flux anomalies primarily follow τ=constant characteristics.

Figure 4. Ice-shelf response can be organized in terms of steady and unsteady behavior using the ξ- and τ-characteristics to partition the x,t plane. In scenario I, for example, the x,t plane is divided into five regions by the four characteristics that emanate from x=0 at the start and end of the ice-

stream discharge episode. Regions I, III and V are in steady state with current ice-stream discharge (for region III, this discharge is greater than for regions I and V); regions II and IV display unsteady conditions.

Figure 4. Ice thickness anomalies driven by periodic fluctuations in ice-stream thickness (top, scenario II) and velocity (bottom, scenario III). Contour intervals are 0.01 non-dimensional units, negative values are contoured with dashed pattern. The ranges of x and t displayed are both 0.0→1.0. Note that maximum h for scenario III occurs downstream of the grounding line.

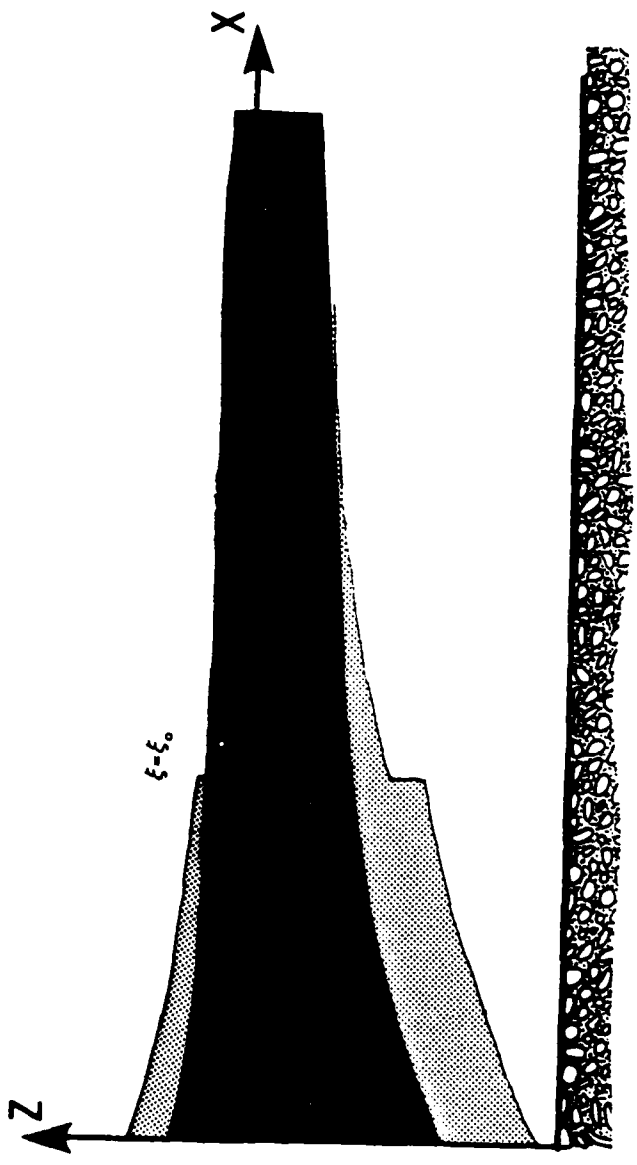

Figure 1

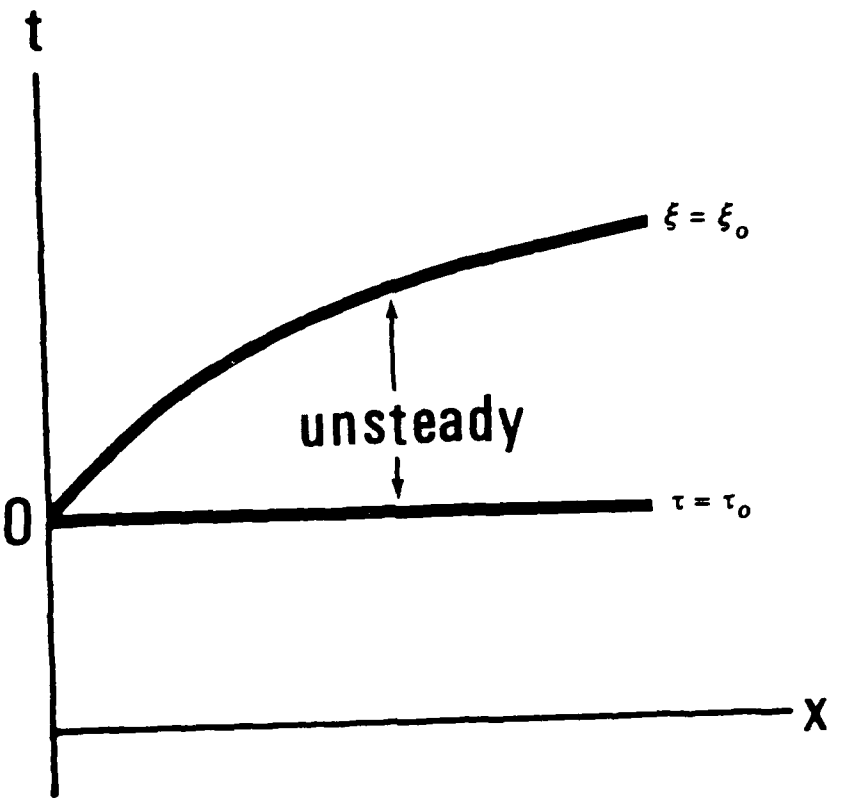

Figure 2

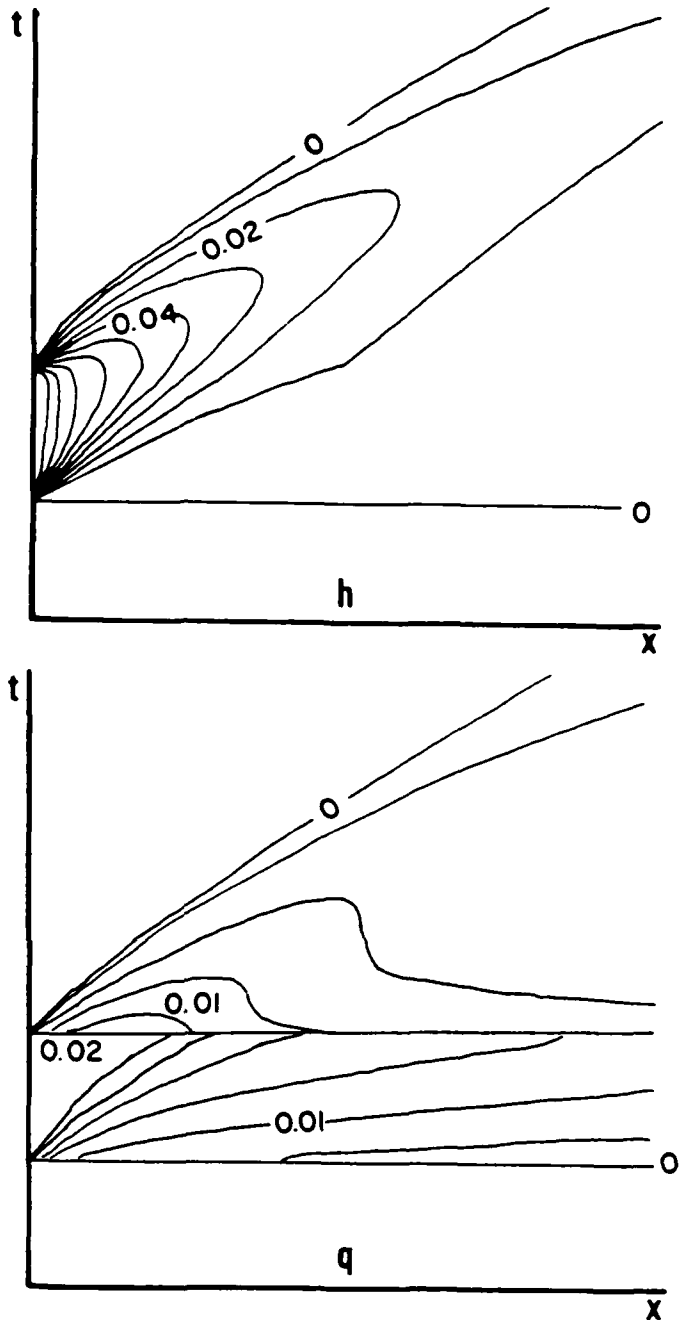

Figure 3

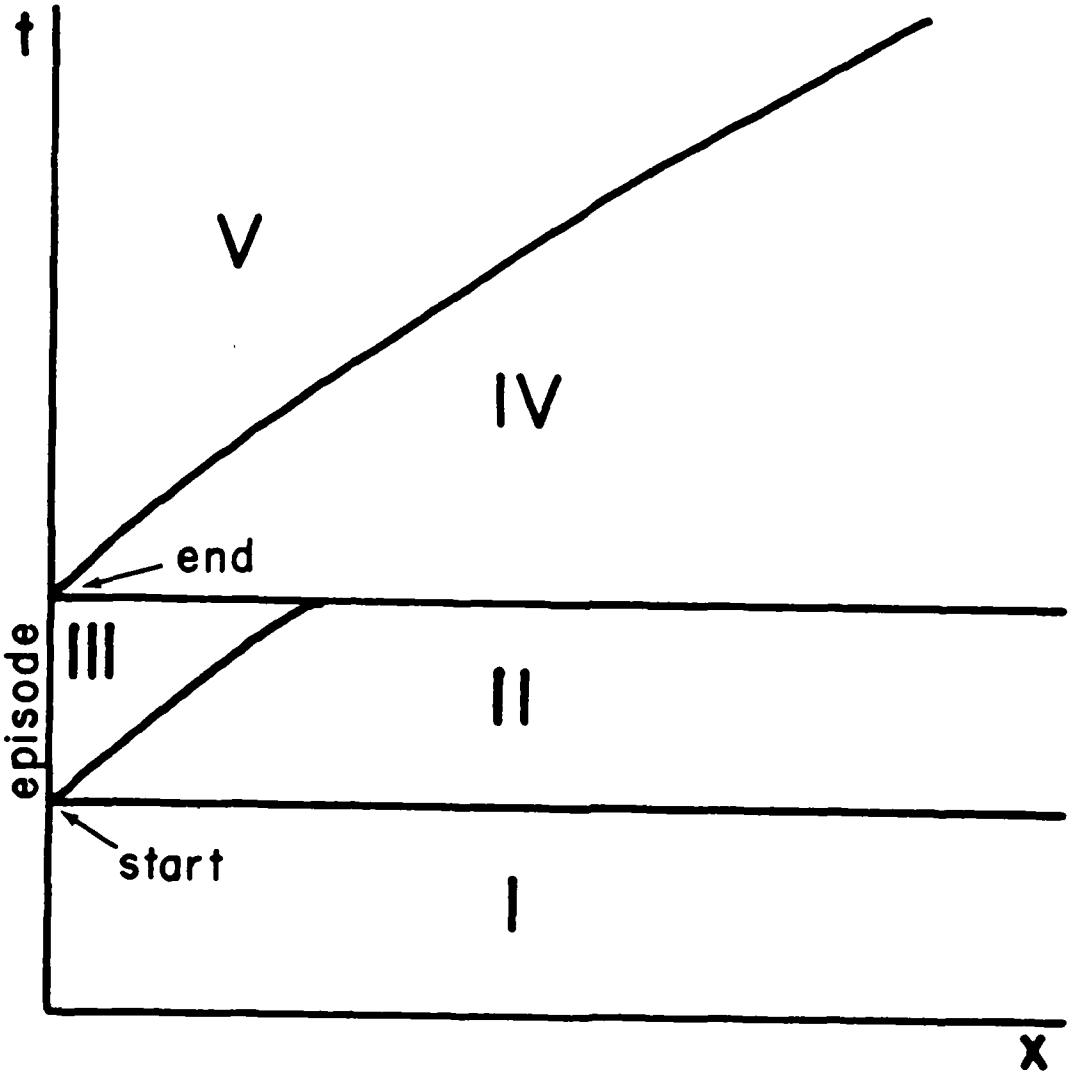

Figure 4

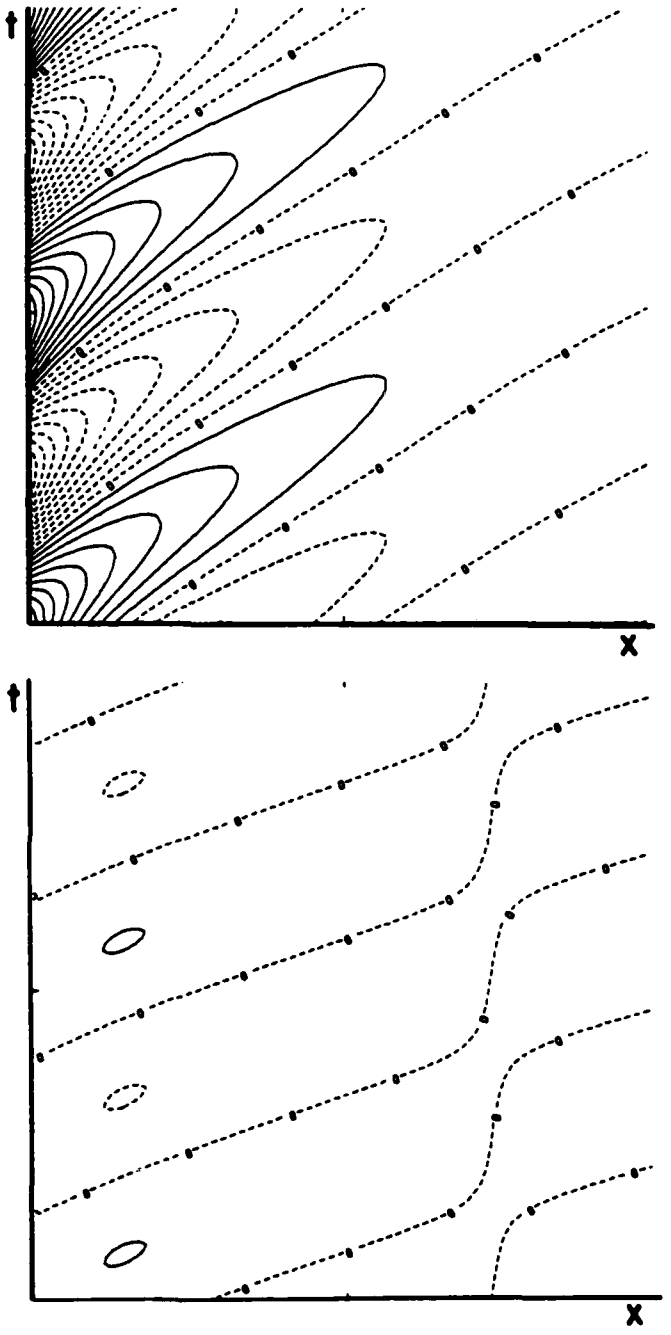

Figure 5

END

DATE

FILMED

3-88

DTIC